JOURNAL OF AIRCRAFT
Vol. 45, No. 5, September–October 2008

Aerodynamic Redesign Using Discrete Adjoint Approach on Overset Mesh System

Byung Joon Lee* and Chongam Kim†
Seoul National University, Seoul 151-744, Republic of Korea

DOI: 10.2514/1.34112

An adjoint-based design approach for the delicate treatment of complex geometry is presented by using an overset mesh technique. Overset blocks, such as collar and tipcap grids, which are commonly used in accurate drag prediction, are employed to evaluate the applicability of the proposed design approach to practical problems. Various pre- and postprocessing techniques for overset flow and sensitivity analyses are implemented to develop a robust gradient-based optimization method on an overset mesh topology. In preprocessing, overlap optimization, which can provide an accurate overset solution and enhance convergence characteristics, is adopted to automatically construct the block connectivity. A new postprocessing method, the spline-boundary intersecting grid scheme, is introduced by reflecting the ratio of the surface cell area for accurate prediction of aerodynamic coefficients and a convenient evaluation of sensitivities under a parallel computing environment. For the sensitivity analysis, the adjoint formulation for the overset boundary condition is implemented in the fully hand-differentiated sensitivity analysis code. A three-dimensional discrete adjoint solver on the overset mesh system is developed by exploiting the overset flow analysis techniques. Good convergence characteristics of the adjoint solver can be achieved by using the automatic construction process of block connectivity. The derivatives of aerodynamic coefficients can be obtained by an efficient and accurate postprocessing technique. The present overset adjoint formulation and flow analysis techniques are validated by comparing the flow and sensitivity analyses, as well as the design results, with those of a single-block case for a transonic wing. Finally, careful designs are carried out by minimizing the drag of a three-dimensional wing–body configuration. The design results successfully demonstrate the capability of the present design approach.

Introduction

GRADIENT-BASED design methods might have difficulties in dealing with highly nonlinear design spaces, where a design solution can often be trapped in the local optimum. Nonetheless, the gradient-based optimization method (GBOM) is still very popular in aerodynamic shape optimization (ASO), because the GBOM is very efficient in finding an optimal shape and it can be readily combined within the multidisciplinary design optimization (MDO) framework. Starting from the earliest adjoint-based ASO [1,2], the interests of ASO via the GBOM have gradually moved into large-scale computations over complex geometries with the rapid progress of the computational environment [3–5]. To deal with complex aircraft geometries, design optimization strategies based on various grid topologies are attracting more and more attention [3–10].

Design on the multiblock grid system can be accomplished by extending the single-block sensitivity module. For example, the multiblock design strategy has been successfully applied to various design problems, such as the drag minimization of wing/body configurations, reduction of sonic boom for supersonic aircraft, optimal shape design of an S-shaped intake, and so on [3–5]. The multiblock grid technique generally secures good grid quality. However, in applications involving moving or deforming grids, which result in a severe grid change or a change in grid topology, it is extremely challenging to realize the fully automatic design only using the multiblock grid system. In the case of the unstructured grid system, the automatic mesh generation is relatively amenable. Thus, unstructured sensitivity analysis codes with the discrete adjoint approach have been developed by Nielsen and Anderson (1998) [6], Kim et al. (2001) [7] and Mavriplis (2007) [8]. Compared with the structured mesh system, however, more grid points are generally required. In addition, memory overhead and computational cost are often inevitable.

On the other hand, the overset grid technique is very attractive in terms of computational accuracy and geometric modeling, which is beneficial to large-scale flow analysis and design optimization. Furthermore, these advantages can be fully exploited to drive the overall aerodynamic design optimization process to the final goal, that is, the fully automatic aerodynamic design from the CAD models.

To implement the adjoint-based sensitivity on the overset mesh system, there are several problems to be resolved. First, convergence characteristics of the adjoint solver are seriously affected by the interpolation error at the overset boundary. This problem becomes more severe in complicated three-dimensional cases where many blocks are overlapped [10]. Second, the objective function has to be fully hand-differentiated at the overlap surface by considering the reconstruction of surface mesh. This may cause a substantial difficulty in an adjoint solver. In addition, the overlap boundaries between the mesh blocks should be treated carefully during the mesh deforming process of design optimization. However, only a few researchers have investigated the studies on ASO using the overset mesh system. Kim et al. performed a two-dimensional multi-element airfoil design with the hand-differentiation of a two-equation turbulence model [9]. In the three-dimensional application, the design of a simple turbine stator vane was performed by Liao and Tsai, which is based on the continuous adjoint approach of the Euler equations using an implicit hole-cutting method [10].

In the present paper, the pre- and postprocessing methods, as well as the adjoint boundary condition, are carefully investigated on the overset mesh system to establish a practical three-dimensional aerodynamic shape design methodology based on the discrete adjoint approach. The spline-boundary interpolation grid (S-BIG) scheme is proposed for efficiently evaluating cell differentiation in

Received 20 August 2007; revision received 14 April 2008; accepted for publication 15 April 2008.

*Postdoctoral Research Fellow, BK21 School for Creative Engineering Design of Next Generation Mechanical and Aerospace Systems. AIAA Member.

†Associate Professor, Corresponding Author, Department of Aerospace Engineering, School of Mechanical and Aerospace Engineering; chongam@snu.ac.kr. AIAA Senior Member.

the adjoint solver. The performance of the overlap optimization technique [11] is investigated in terms of convergence of the adjoint solver and accuracy of the flow solver. By exploiting these techniques, practical drag minimizations of aircraft configurations are successfully carried out on the overset grid system.

Numerical Background

Overlap Optimization for the Flow and Sensitivity Analysis

The capability of the adjoint-based ASO on the complex overset mesh system depends critically on the performance of the preprocessor. Regarding the flow analysis techniques on the overset mesh system, continuous progress has been made. One of the primary concerns in this field is developing a robust and efficient preprocessor. Several high-quality processors, such as PEGASUS [11], DCF3D [12], BEGGAR [13,14], and Overture [15], have been developed. PEGASUS, especially, is regarded as one of the most efficient and robust preprocessors. It has been applied to high-fidelity flow simulations, including flow analyses over various full-body aircraft, spacecraft, and so on [11]. To allow the complex overset mesh system with a huge number of blocks and complicated block connectivity, a process for finding hole points and constructing block connectivity automatically is the key step, which is known as the overlap optimization [11]. By interpolation via cell difference parameter [11], which considers the cell volume ratio and the cell aspect ratio between donor and fringe cells, overlap optimization can also contribute to the convergence characteristic of flow analysis codes. In addition, it can reduce numerical oscillation by minimizing the overlap computational domain. Based on this observation, overlap optimization is extended to the sensitivity analysis module to improve the convergence and accuracy characteristics.

Figure 1 shows the overset computational domains around the fuselage of a wing/body configuration. Figure 1a is the computational region in which the block connectivity is assigned manually, and Fig. 1b is the overlap optimization case. The overlap computational region where two or more meshes coexist is minimized by overlap optimization. In the case of Fig. 1a, the difference in the computed solutions in the overlap (but not optimized) computational domain may trigger an error in fringe cell interpolation, which leads to a serious convergence problem. Figures 2a and 3a demonstrate this difficulty. On the other hand, the computed result obtained by overlap optimization, as given in Figs. 2b and 3b, does not exhibit such behavior. Because a sufficient convergence of the flow solution is a prerequisite for the convergence of an adjoint solution, overlap optimization is essential to the adjoint solver. Figure 4 compares the convergence characteristics of the adjoint code with and without overlap optimization. For the ONERA-M6 wing with the two-block overset mesh system, manual hole cutting and donor cell search routines do not provide a stable convergence of the overset adjoint solver. By the overlap optimization, a satisfactory convergence can be obtained even in the DLR-F4 wing/body configuration with the seven-block overset mesh system.

Spline-Boundary Intersecting Grid Scheme

To calculate the aerodynamic coefficients in overset flow analysis, the zipper grid scheme [16] is widely used. The zipper grid is a kind of grid reconstruction method. This method consists of two steps: the blanking process of the overlap computational region, and the reconstruction process of the overlap region with a set of unstructured grids. The flow variables on the zipper grid are then interpolated from the donor cells of the original overlap region. In this case, the numerical differentiation of the flux terms on the zipper

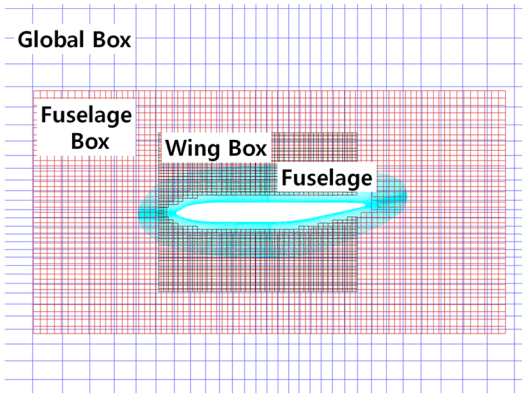

a) Manually assigned fringe boundary

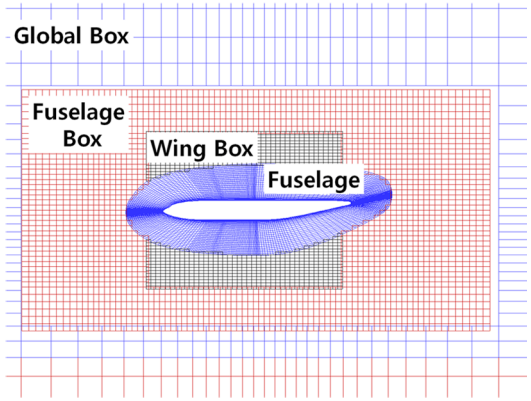

b) Overlap optimized fringe boundary

Fig. 1 Comparison of computational domains.

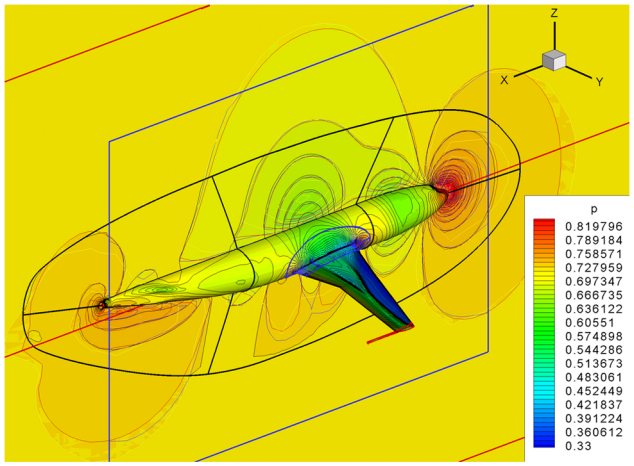

a) Manually assigned fringe boundary

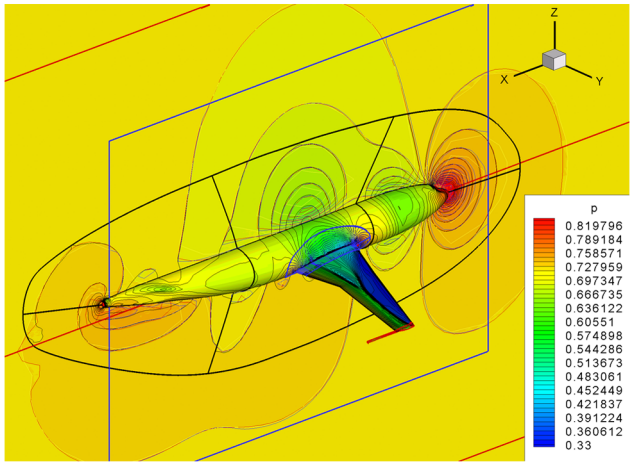

b) Overlap optimized fringe boundary

Fig. 2 Comparison of flow analysis results (pressure contours).

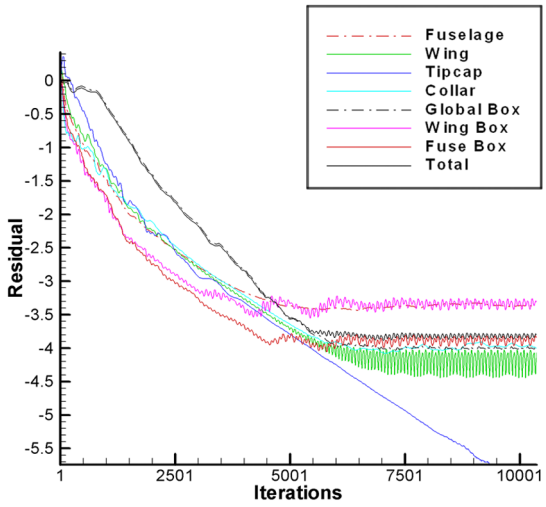

a) Manually assigned fringe boundary

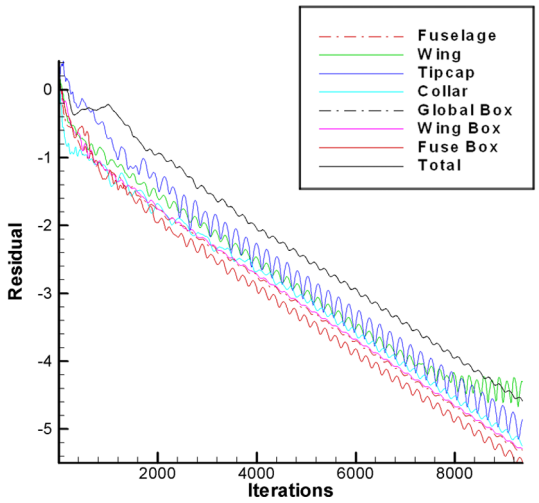

b) Overlap optimized fringe boundary

Fig. 3 Comparison of flow analysis results (convergence characteristics).

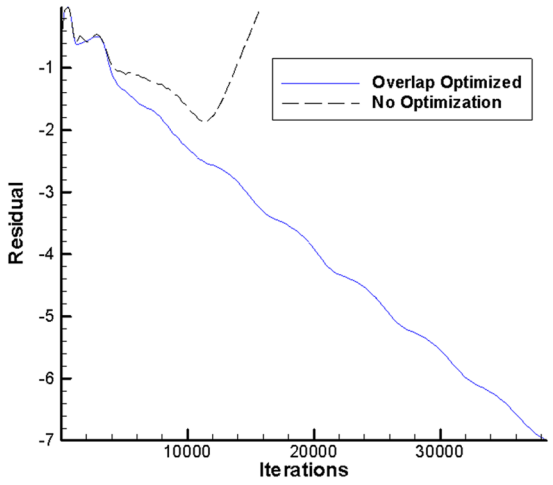

a) 2 block system (ONERA-M6 wing)

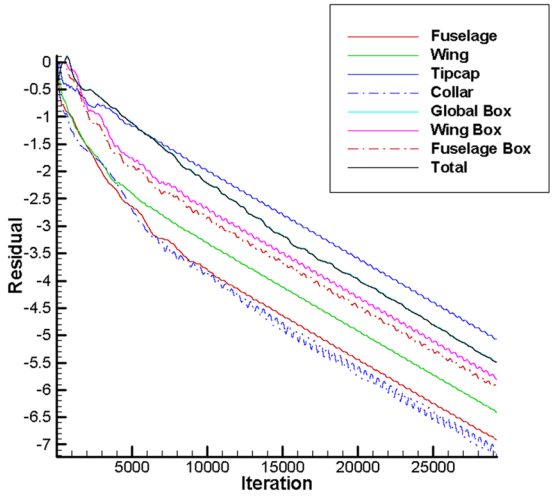

b) 7 block system (DLR-F4)

Fig. 4 Residual history of overlap optimized adjoint solver [Courant–Friedrichs–Lewy (CFL) no. = 1.5].

grid, which is necessary in the adjoint code, is quite difficult and inefficient. Thus, the S-BIG scheme has been newly devised, and it is applied to the postprocessing and sensitivity analyses routines. The purpose of the S-BIG scheme is to evaluate aerodynamic coefficients without interpolating flow variables from donor cells. As a result, to numerically differentiate the flux terms or to evaluate aerodynamic coefficients, the S-BIG scheme does not require anything except the boundary information of the overlap region.

Reorganization of Cutcell

The S-BIG scheme is composed of four steps. In the first step, the boundaries of the overlap region have to be determined. For the interface between the fuselage and the collar block, the outer boundary of the collar block is chosen, as shown in Fig. 5. The interface on the wing surface, such as the collar–wing or the wing–tipcap boundary, can be simply specified by a constant line ($y = \text{const}$). The chosen boundary is then parameterized by the B-spline function.

The next step is to divide the surface grid points into inner or outer vertices according to the prescribed spline boundary. After blanking each vertex appropriately (NBLANK = 1 for the outer vertex, and NBLANK = 0 for the inner vertex), there are a total of 16 cases, as shown in Fig. 6. As in the case of the conservative chimera scheme [17], surface cells can be classified into three types of cells (normal, cut, and hole) according to the number of blanked vertices. Next, the intersection points between the spline boundary and the four edges of

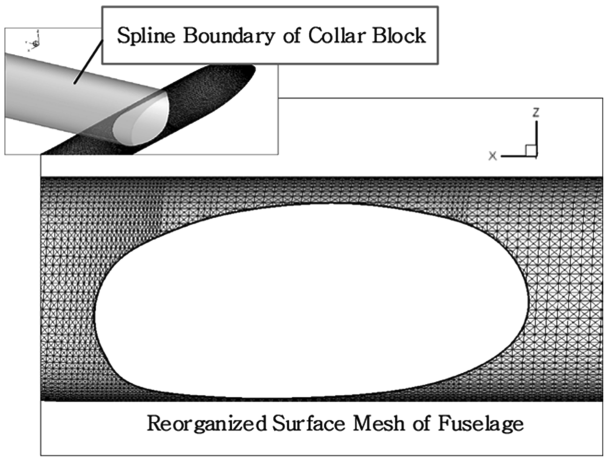

Fig. 5 Spline boundary of collar block at the interface with fuselage surface.

the cutcell are determined, and the blanked area of the cutcell is removed. Finally, the cutcell is reorganized into a number of triangles by simply connecting the cell center point with the vertices and intersection points. Figure 7 shows an example for case 2. The other cases (3–15) can be done similarly.

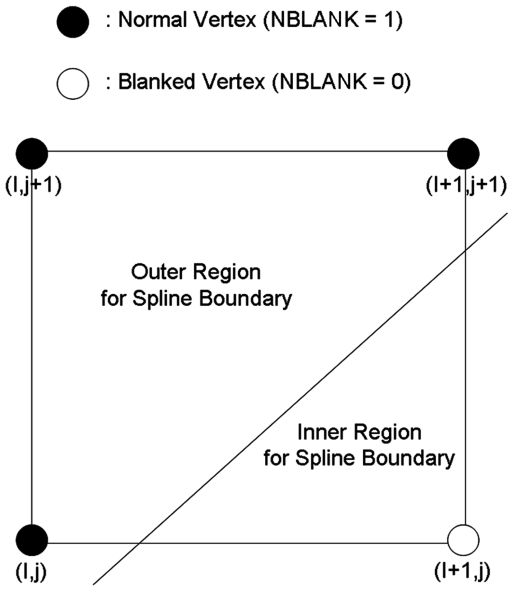

a) Blanking process by spline boundary

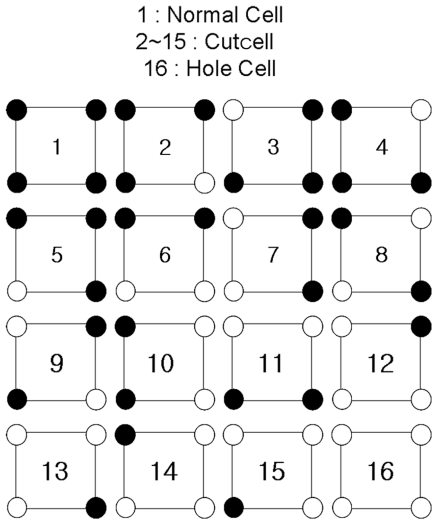

b) Type of blanked surface cell

Fig. 6 Type of surface cell.

Extra Triangle for Error Correction/Integration of Aerodynamic Coefficients

When the boundary is curved like the fuselage–collar interface, the reorganized cutcell has to be modified to accurately calculate aerodynamic coefficients. As shown in Fig. 8, an extra triangle, composed of two intersection points and a curved boundary point, is added (or subtracted) to the reorganized cutcell.

Finally, aerodynamic coefficients are calculated by simply summing up the aerodynamic coefficients of each triangle in the reorganized cutcell. Figure 9 shows the reorganized surface grids by the S-BIG scheme near the fuselage–collar block interface for the DLR-F4 configuration.

Adjoint Formulation for Overset Boundary

The discrete adjoint variable method is applied to get sensitivity information by fully hand-differentiating the three-dimensional Euler equations. The discrete residual of the governing equations $\mathbf{R}$ is a function of the flow variable vector $\mathbf{Q}$, the position of the computational grid $\mathbf{X}$, and the vector of the design variables $\mathbf{D}$. Similarly, the aerodynamic objective function F also depends on $\mathbf{Q}$, $\mathbf{X}$, and $\mathbf{D}$. The differentiations of $\mathbf{R}$ and F are then combined by the adjoint vector Λ [5–9]. During this procedure, the sensitivity

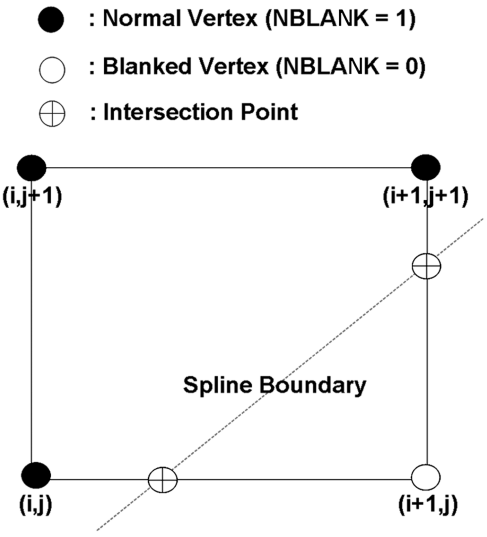

a) Initial blanked cutcell

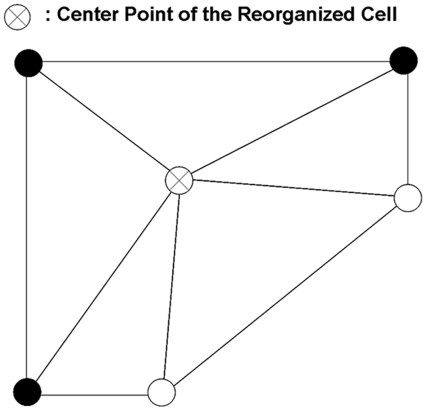

b) Reorganized cutcell

Fig. 7 Reorganization of cutcell.

derivative can be efficiently calculated without evaluating $\{\mathrm{d}\mathbf{Q}/\mathrm{d}\mathbf{D}\}$ as

$$\left\{\frac{\mathrm{d}F}{\mathrm{d}\mathbf{D}}\right\} = \left\{\frac{\partial F}{\partial \mathbf{X}}\right\}^T \left\{\frac{\mathrm{d}\mathbf{X}}{\mathrm{d}\mathbf{D}}\right\} + \left\{\frac{\partial F}{\partial \mathbf{D}}\right\} + \Lambda^T \left(\left[\frac{\partial \mathbf{R}}{\partial \mathbf{X}}\right] \left\{\frac{\mathrm{d}\mathbf{X}}{\mathrm{d}\mathbf{D}}\right\} + \left\{\frac{\partial \mathbf{R}}{\partial \mathbf{D}}\right\} \right) \tag{1}$$

if and only if the adjoint vector Λ satisfies the following adjoint equation:

$$\left[\frac{\partial \mathbf{R}}{\partial \mathbf{Q}}\right]^T \Lambda + \left\{\frac{\partial F}{\partial \mathbf{Q}}\right\} = \{0\}^T \tag{2}$$

The solution vector Λ is then obtained by solving Eq. (2) with the Euler implicit method in a time-iterative manner as

$$\left(\frac{I}{J\Delta t} + \left[\frac{\partial \mathbf{R}}{\partial \mathbf{Q}}\right]_{\mathrm{VL}}^T\right)\Delta\Lambda = -\left[\frac{\partial \mathbf{R}}{\partial \mathbf{Q}}\right]^T \Lambda^m - \left\{\frac{\partial F}{\partial \mathbf{Q}}\right\}^T, \qquad \Lambda^{m+1} = \Lambda^m + \Delta\Lambda \tag{3}$$

where I is the identity matrix, J is the Jacobian matrix, and the subscript VL indicates the Van Leer flux Jacobian. Adjoint formulation on the overset boundary can be derived by slightly modifying the conventional discrete adjoint boundary condition. The boundary conditions can be expressed as

$$\left[\frac{\partial \mathbf{R}^M}{\partial \mathbf{Q}^M}\right]^T \Lambda^M + \left[\frac{\partial \mathbf{R}_F^S}{\partial \mathbf{Q}^M}\right]^T \Lambda_M^S + \left\{\frac{\partial F^M}{\partial \mathbf{Q}^M}\right\}^T = \{0\}^T \tag{4}$$

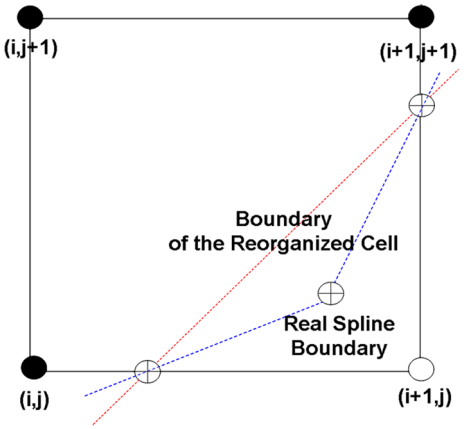

a) Concave type spline boundary

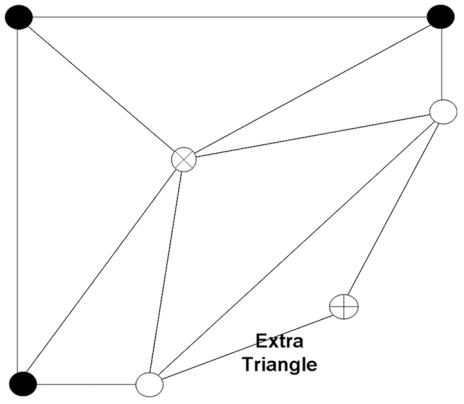

b) Addition of extra triangle

Fig. 8 Extra triangle for cutcell.

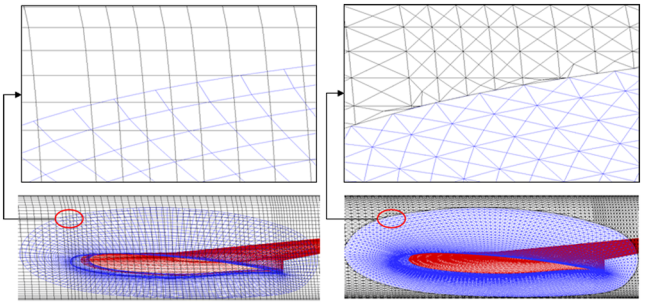

Fig. 9 Reconstructed surface mesh of DLR-F4 wing/body configuration (left: original overset mesh, right: reorganized mesh by S-BIG).

$$\left[\frac{\partial \mathbf{R}^S}{\partial \mathbf{Q}^S}\right]^T \Lambda^S + \left[\frac{\partial \mathbf{R}_F^M}{\partial \mathbf{Q}^S}\right]^T \Lambda_F^M + \left\{\frac{\partial F^S}{\partial \mathbf{Q}^S}\right\}^T = \{0\}^T \tag{5}$$

$$\left[\frac{\partial \mathbf{R}^M}{\partial \mathbf{Q}_F^M}\right]^T \Lambda^M + \left[\frac{\partial \mathbf{R}_F^M}{\partial \mathbf{Q}_F^M}\right]^T \Lambda_F^M + \left\{\frac{\partial F^M}{\partial \mathbf{Q}_F^M}\right\}^T = \{0\}^T \tag{6}$$

$$\left[\frac{\partial \mathbf{R}^S}{\partial \mathbf{Q}_F^S}\right]^T \Lambda^S + \left[\frac{\partial \mathbf{R}_F^S}{\partial \mathbf{Q}_F^S}\right]^T \Lambda_F^S + \left\{\frac{\partial F^S}{\partial \mathbf{Q}_F^S}\right\}^T = \{0\}^T \tag{7}$$

where the subscript F indicates a fringe cell. The superscript M and S represent the main and subgrid domains, respectively. By solving the four equations sequentially, the overset boundary values on the main and subgrid domains can be updated. For the subgrid domain, the fringe cell value of the main grid Λ_F^M is first updated from the inner cell value of the main grid Λ^M using Eq. (6). The inner cell value of the subgrid Λ^S is then updated from the fringe cell value of the main grid Λ_F^M as in Eq. (5). For the main grid domain, Eqs. (4) and (7) are used in a similar manner. The fringe cell value of the subgrid Λ_F^S is updated from the inner cell value of the subgrid Λ^S using Eq. (7). The inner cell value of the main grid Λ^M is finally updated from the fringe cell value of the subgrid Λ_F^M from Eq. (4).

The update procedure of the adjoint variables on the overset boundary is simply the reverse of the flow analysis because of the transposed operation in the adjoint formulation.

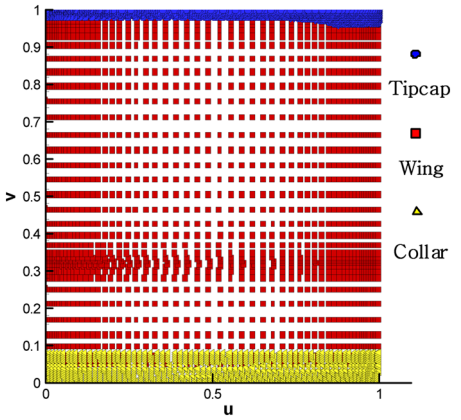

Fig. 10 Overset mesh transformed onto the planform domain (u-v coordinate).

Shape Modification of Overlap Surface

To efficiently deform meshes on the overlap surface during the design process, a mapping technique from the physical (x-y coordinate) to the planform domain (u-v coordinate) is introduced. The mapping between the two domains can be defined by

$$u = (y - y_{\text{root}})/B, \qquad v = [x_{\text{TE}}(y) - x]/c(y) \tag{8}$$

where B is the wingspan, $c(y)$ is the chord length, and $x_{\text{TE}}(y)$ is the x coordinate of the trailing edge at the wing section y. As shown in Fig. 10, the overlap block surface of the wing, such as the collar–wing and wing–tipcap blocks, can be represented through the mapping relationship by distributed vertices with values between 0 and 1 in the u-v plane. Once the mapping between the two domains is suitably defined, as in Eq. (8), a suitable function f, such as the Hick–Henne function or the B-spline function, can be employed to carry out flexible shape deformation. After the mapping, the final modified overlap surface can be obtained by simply superposing the deformation function over the baseline model:

$$z(u, v) = z_b(u, v) + f(u, v) \tag{9}$$

where the subscript b represents the geometry of the baseline model. The grid sensitivity is then easily evaluated from the sensitivity of the deformation function as

$$\left.\frac{\partial z}{\partial \beta_k}\right|_{u,v} = \left.\frac{\partial f}{\partial \beta_k}\right|_{u,v} \tag{10}$$

Figure 11 shows the deformed meshes of the overlap block surface after the mapping process.

Flow Analysis

Test Cases and Overset Mesh Systems

For design optimization, two test geometries are considered. A two-block system of the ONERA-M6 wing is used to validate the overset flow solver and the adjoint sensitivity code. The mesh system consists of a wing block ($143 \times 39 \times 33$) and a global box block ($63 \times 27 \times 63$). The wing block is constructed with an O-O type

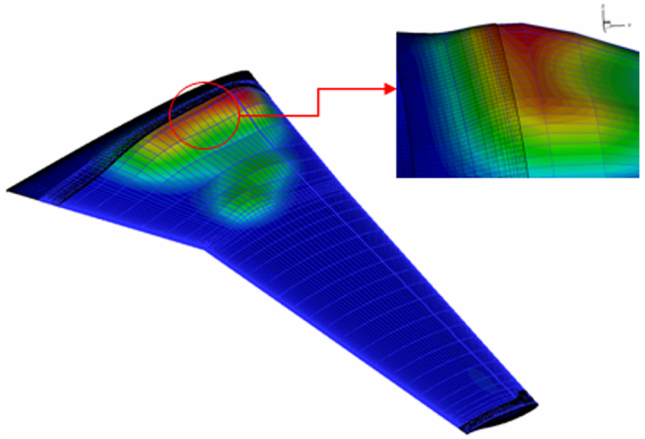

Fig. 11 Deformation of surface mesh at the overset block interface.

grid, whereas the box grid is a Cartesian grid, as shown in Fig. 12a. The number of mesh points is about 300,000.

The DLR-F4 wing/body configuration, which was the test geometry in the first Drag Prediction Workshop (DPW-I), is adopted for practical aerodynamic shape design and large-scale computation [18,19]. Figure 12b shows the overall mesh system, which is composed of seven blocks: a global box ($77 \times 38 \times 72$), a fuselage box ($84 \times 26 \times 45$), a wing box ($44 \times 37 \times 54$), a fuselage block ($190 \times 41 \times 30$, O-O type), a collar block ($146 \times 26 \times 26$, O-H type), a wing block ($143 \times 43 \times 34$, O-H type), and a tipcap block ($103 \times 43 \times 42$, C-type). All the box blocks are simple Cartesian grids. The total number of mesh points is about 1.22 million. To provide a high-quality mesh, the collar block is added at the junction of the wing and fuselage, and the tipcap block is also added around the wing tip. The fuselage block is a single-block mesh system based on an untrimmed approach [20].

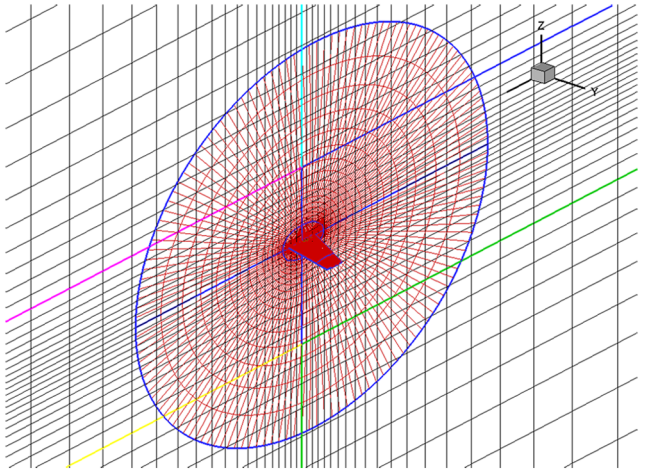

a) ONERA-M6 wing (2 Blocks)

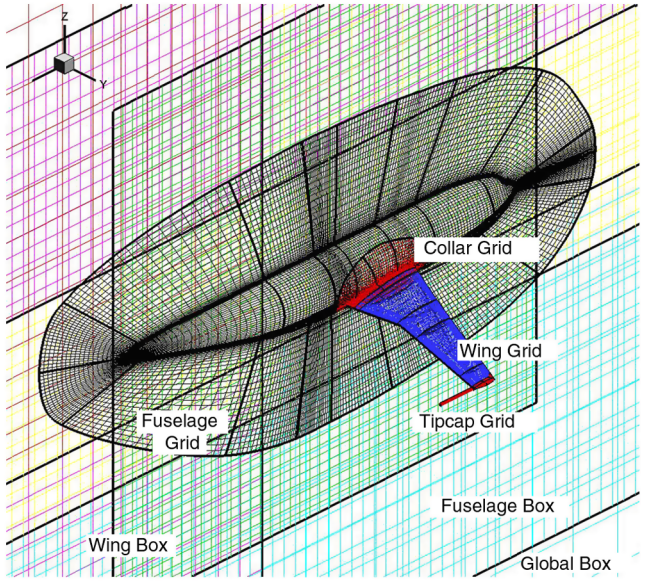

b) DLR-F4 (7 Blocks)

Fig. 12 Overset mesh system for the design works.

Flow Conditions and Numerical Techniques

The flow condition of the ONERA-M6 wing is a well-known case in which a Λ shock appears on the wing surface: a freestream Mach number of 0.84 and an angle of attack of 3.06 deg. In the case of the DLR-F4, the freestream Mach number is 0.75 and the angle of attack is 0.0 deg, which corresponds to the cruising condition.

The three-dimensional compressible Euler equations are transformed into generalized coordinates and are solved with the finite-volume method. To calculate the residual, convective terms are upwind-differenced based on the RoeM scheme by Kim et al. [21] A MUSCL approach using a third-order interpolation is used to obtain a higher order of spatial accuracy in all calculations. For temporal integration, the LU-SGS scheme is used [22].

Validation of Overset Flow Analysis

In general, the trilinear interpolation at the overlap block boundary does not satisfy the conservation property, which may deteriorate the

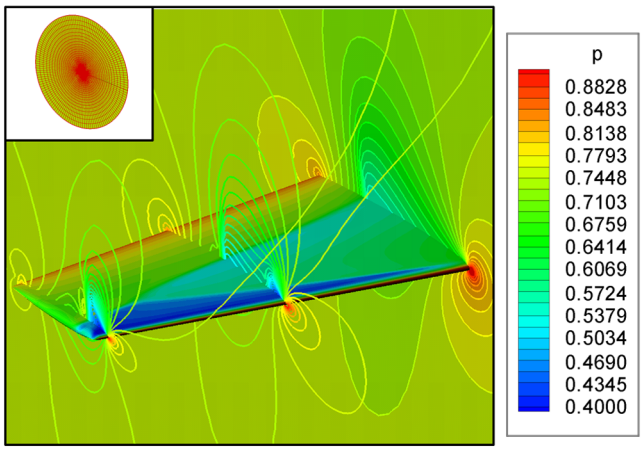

a) Single block system

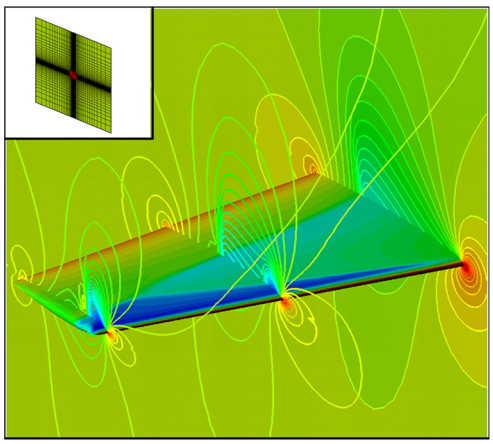

b) Overset mesh system (2 Blocks)

Fig. 13 Pressure contours [ONERA-M6, $M = 0.84$, angle of attack (AOA) $= 3.06$ deg].

accuracy of computations. To examine this for the problems of current interests, the computed results obtained by the overset flow solver are compared with the single-block calculation for the transonic flow over the ONERA-M6 wing. Especially, the shock position and the strength of expansion waves at the leading edge are examined. Overlap optimization is applied, and the position of the hole–fringe boundary is sufficiently far away from the shock wave and wing surface. Figure 13 shows the pressure field around the wing surface. The pressure distribution obtained from the overset flow solver coincides with the single-block solutions almost exactly. The computed results of the DLR-F4 geometry with the seven-block overset system are also obtained by the same overset flow solver. As shown in Figs. 13 and 14, good convergence characteristics of aerodynamic coefficients as well as residual histories are obtained, and a strong Λ shock can also be seen.

From all the results, it can be seen clearly that the present overset flow solver provides sufficient performance to deal with transonic aerodynamic analysis around an airplane configuration.

Sensitivity Analysis and Design Optimization

Validation of Sensitivity Analysis

The design variables used to validate the overset adjoint code are 20 Hicks–Henne functions at each design section of the ONERA-M6 wing. Ten Hicks–Henne functions are equally distributed on the upper and lower surfaces, respectively [23]. The total number of design variables is 60, and geometric modification is performed at the three design sections of wing root, midpoint, and wing tip. The values at other sections are linearly interpolated from the three sections.

In Fig. 15, the sensitivity values of the drag coefficient obtained from the overset adjoint solver are compared with the results of the single-block case and complex step derivative (step size 10^{-8}). The results of the complex step derivative are obtained from the complex form of the overset flow solver [24]. The complex step derivative and the adjoint solver provide almost the same results within a 1–2% margin of error. In addition, the sensitivities from the single-block and overset adjoint solvers coincide very well with each other for most of the design variables. In the upper wing surface (10th–20th design variables), the difference in the gradient values becomes relatively larger due to the nonlinear flow characteristic originating from the shock wave. Because a different design solution can be obtained even with this small difference, the design results from the single-block and overset mesh systems are compared in the next section.

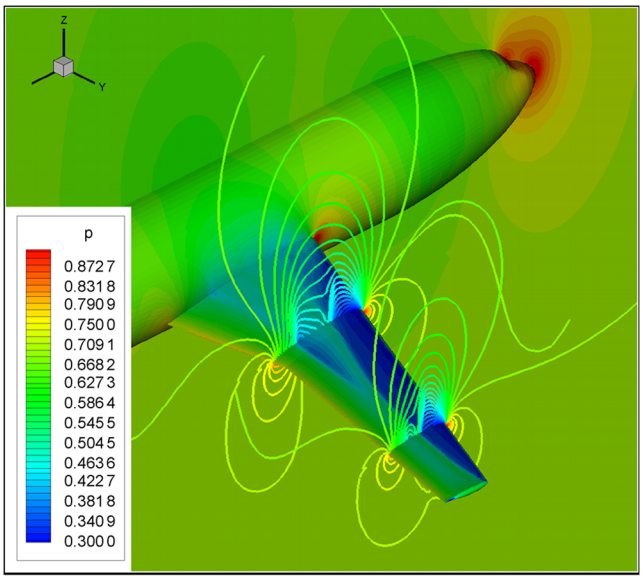

a) Pressure contour

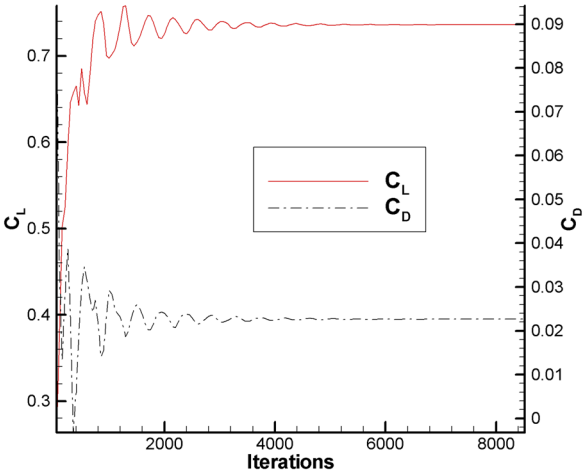

b) Convergence history of aerodynamic coefficients

Fig. 14 Flow analysis results of wing/body configuration (DLR-F4, $M = 0.75$, AOA $= 0.0$ deg).

Drag Minimization

The present overset design approach is applied to design optimization of transonic wing and wing/body configurations. Optimization is performed using the Broydon-Fletcher-Goldfarb-Shanno (BFGS) variable metric method, which is a kind of nonconstrained optimization technique [25]. As a standard application of the overset GBOM tool, a drag minimization of the transonic ONERA-M6 with a constant lift coefficient is first performed. The number of design variables and all of the flow conditions are the same as in the flow validation case. The objective function is defined by Eq. (12) with the constraint of Eq. (11). To balance the variation of the objective and penalty functions, the weighting factor of the lift constraint is given by the ratio of the lift sensitivity to that of the drag with respect to the angle of attack:

Minimize C_D, subject to

$$C_L = C_{L_0} \tag{11}$$

where C_{L_0} is the lift coefficient of the baseline model.

$$F = C_D + Wt \times \min[0, C_L - C_{L_0}], \qquad Wt = \frac{\partial C_D/\partial \alpha}{\partial C_L/\partial \alpha} \tag{12}$$

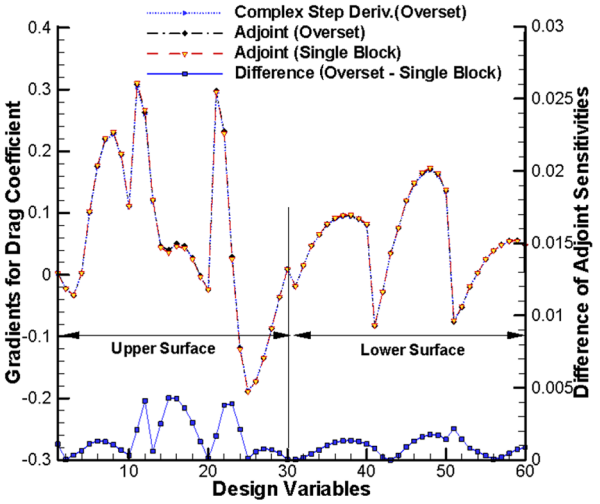

Fig. 15 Validation of sensitivity analysis code.

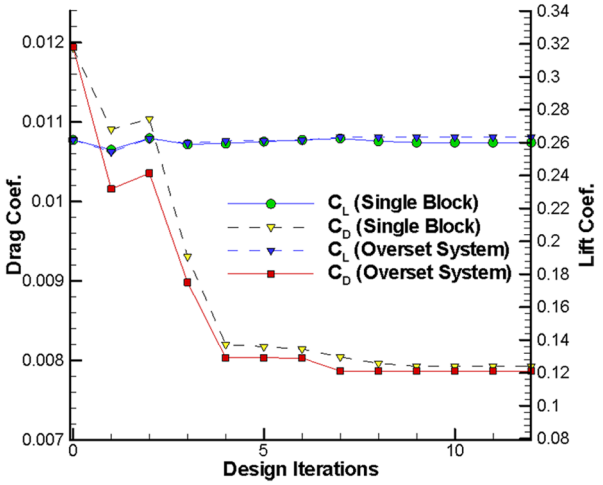

Fig. 16 Design history (ONERA-M6 wing design).

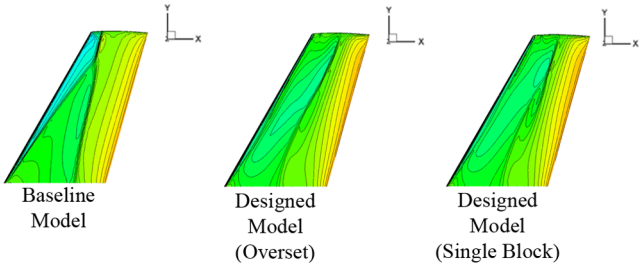

Fig. 17 Comparison of surface pressure distribution.

Transonic Wing Design

The performance of the overset GBOM tool is investigated through a comparison with the single-block design results. Regarding the overset design results, the drag coefficient is remarkably reduced during the design process, as shown in Fig. 16. The design process converges well and the drag coefficient decreases from 0.0119 to 0.0079 (32% reduction) after 15 design iterations, whereas the lift coefficient almost remains at the initial value of 0.2600. L/D is changed from 22.37 to 32.90 (47% increase). The pressure distributions of the baseline ONERA-M6 and designed wings are compared in Fig. 17. It is observed that the strong Λ shock on the wing upper surface has diminished considerably. The C_P curve at each section of the designed wing shows that the flow acceleration right after the leading edge is somewhat mitigated, owing to the shape change of the wing nose. As a result, the wave drag on the upper surface is considerably reduced.

Figure 16 compares the overset design result with the single-block case. The overall design histories are essentially the same with each other. Some discrepancies can be observed at the initial design stage, which may be caused by the sensitivity difference around the shock wave of the baseline geometry, as shown in Fig. 15. After a few design iterations, the strength of the initial shock wave in both designs becomes weaker in a similar manner, and the afterward design iterations follow almost the same path. The pressure distributions on the upper wing surface are compared in Fig. 17. The flow pattern of both designed wings is very similar to the other. In the midspan region, however, some pressure difference can be observed, which can also be seen in the C_p distribution and wing section geometry in Figs. 18 and 19.

Judging from the comparisons, the design process based on the single-block and overset mesh systems provides almost the same result. Consequently, the loss of accuracy in the flow and sensitivity analyses, which is caused by the nonconservative interpolation at the overlap block boundary, can be properly avoided by keeping the hole–fringe boundary away from the shock wave and wing surface. However, further studies, including an efficient implementation of the conservative overset mesh system or an accurate interpolation scheme at the overset boundary, are necessary to eliminate the error.

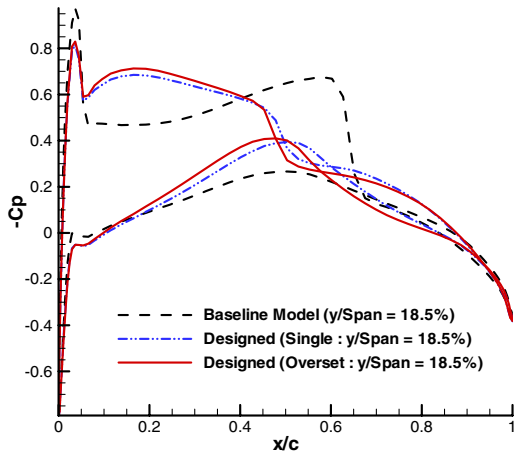

a) Wing root

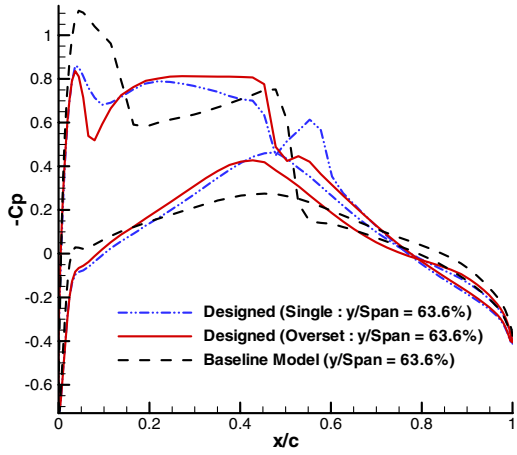

b) Midspan

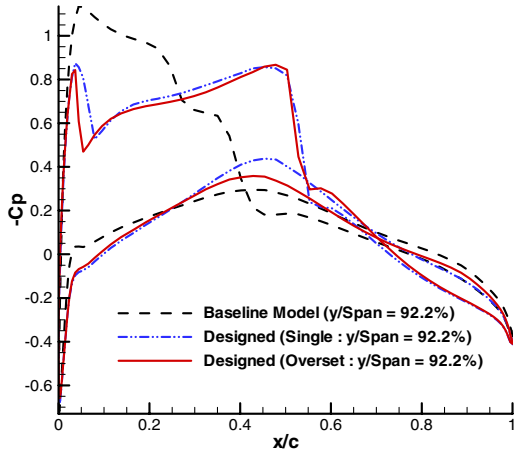

c) Wing tip

Fig. 18 Comparison of C_P curves (ONEAR-M6 wing design).

Redesign of DLR-F4 Wing/Body Configuration

As a more complicated design work, the DLR-F4 wing/body configuration using seven blocks of the overset mesh system is considered. The total number of design variables is 200 at 10 different design sections of the wing surface. At each design section,

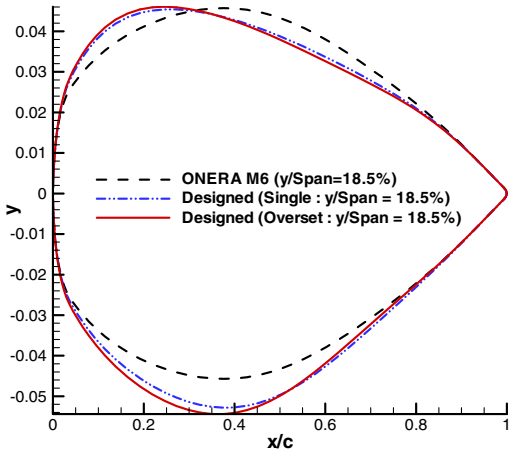

a) Wing root

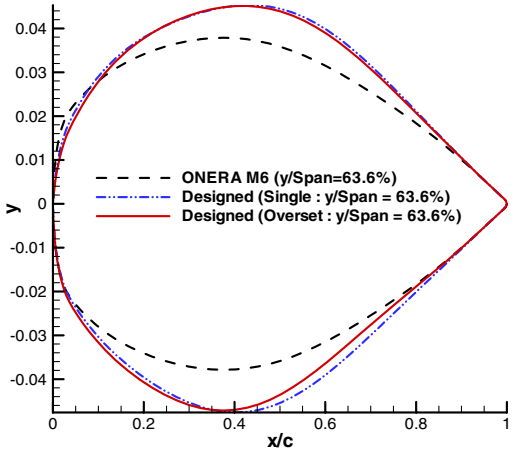

b) Midspan

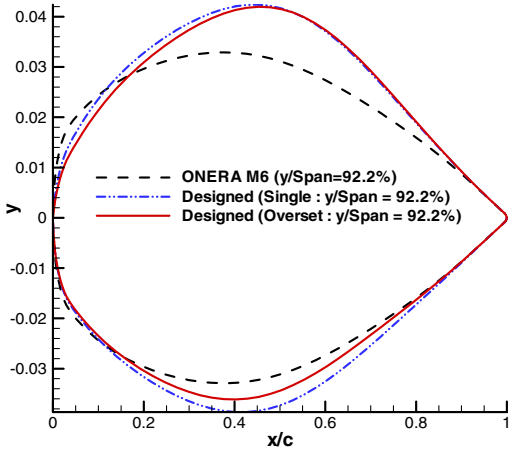

c) Wing tip

Fig. 19 Comparison of geometric change (ONEAR-M6 wing design).

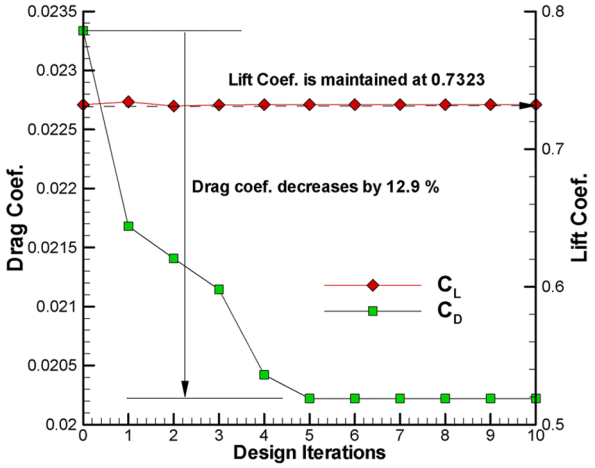

Fig. 20 Design history (redesign of DLR-F4 wing/body configuration).

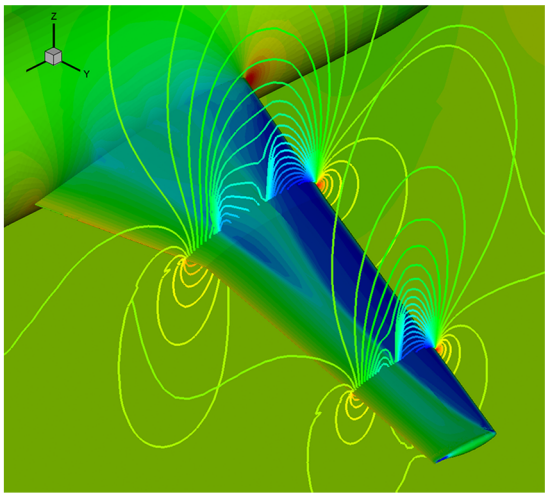

a) Baseline model (DLR-F4)

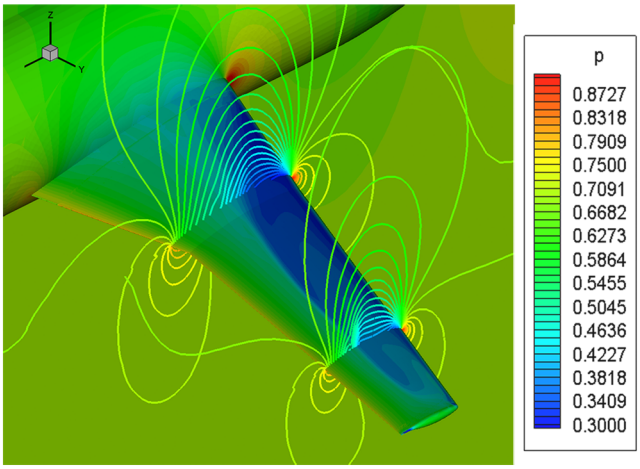

b) Designed model

Fig. 21 Comparison of flow pattern between the baseline model and the designed model (redesign of DLR-F4 wing/body configuration).

20 Hicks–Henne functions are used, as in the case of the ONERA-M6 wing design. Three component blocks (collar, wing, and tipcap) are overlapped on the wing surface. The deformation of the overlap surface meshes is carried out by the mapping technique from the wing surface to the planform domains. The design history in Fig. 20 shows that the drag coefficient decreases from 0.0227 to 0.0202 (12% reduction) after 10 design iterations. Taking into account the drag portion of the fuselage, this seems to be quite reasonable because the drag reduction for the wing only is about 17%. The L/D increases from 32.26 to 36.25 (12.3%). It can be observed in Fig. 21 that the shock strength on the wing surface is remarkably diminished after the design. At the 33% wingspan section, as shown in Figs. 22a and 23a, the front shock on the upper surface almost disappears

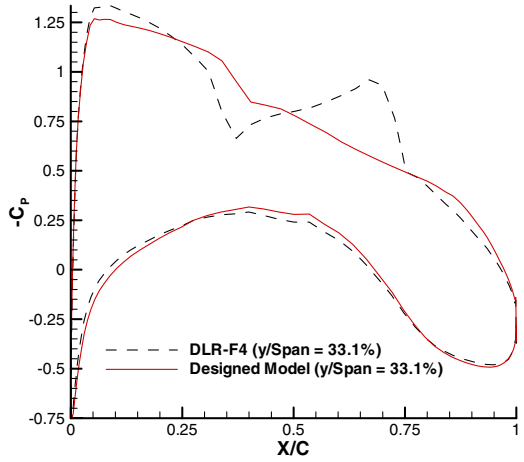

a) Wing root

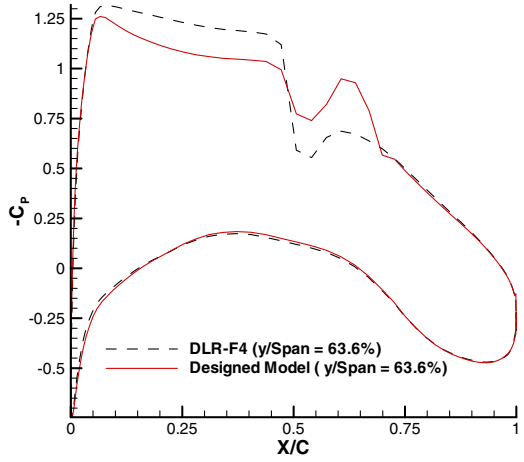

b) Midspan

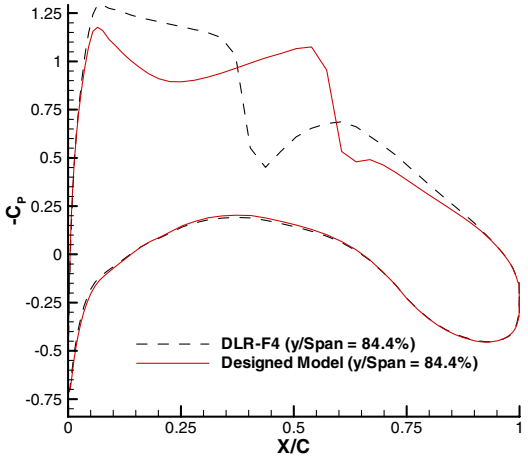

c) Wing tip

Fig. 22 Comparison of C_P curves (redesign of DLR-F4 wing/body configuration).

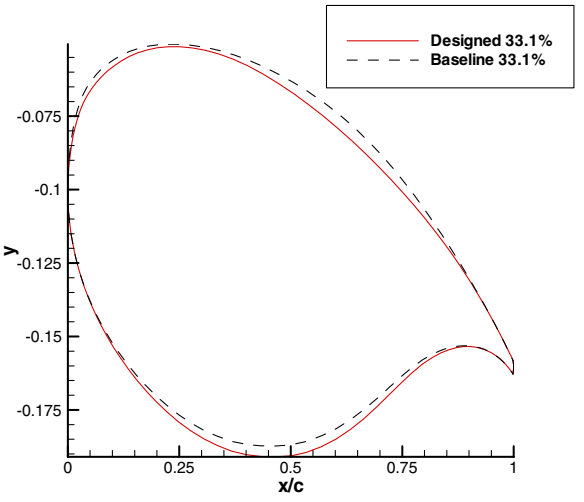

a) Wing root

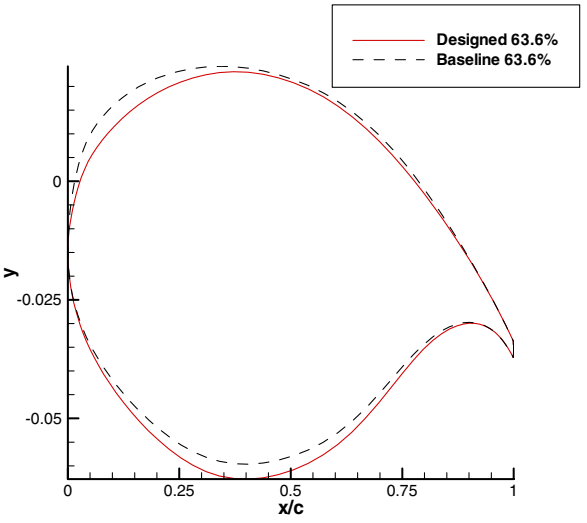

b) Midspan

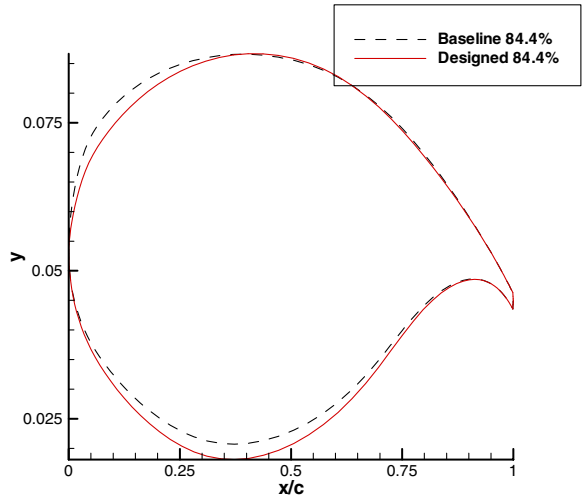

c) Wing tip

Fig. 23 Comparison of geometric change (redesign of DLR-F4 wing/body configuration).

because the shelving leading edge relieves a strong flow expansion. As for the rear shock, the relatively mild slope around $x/c = 75\%$ prevents a drastic flow expansion after the front shock. The maximum thickness of the wing section is not changed to satisfy the lift constraint. As shown in the 63.6 and 84.4% wingspan sections in Figs. 22 and 23, the position of the maximum thickness along the spanwise direction shifts toward the trailing-edge region due to the twist angle of the baseline wing. Thus, after the maximum thickness, there is no sufficient flow region to change the rear shock wave into gradual compression waves. Furthermore, the geometric change in

the upper wing surface after the maximum thickness region is very limited as the wing section gets closer to the wing tip. To obtain more refined design solutions, such as a shock-free wing, planform design variables including the twist angle need to be incorporated. However, with the present design tool based on the discrete adjoint approach and the overset mesh system, the designed wing shows substantially enhanced aerodynamic characteristics, which demonstrates the capability of the proposed approach in the design of a complicated three-dimensional configuration.

Conclusions

An optimal shape design approach based on discrete adjoint formulation and the overset mesh technique is carefully discussed. The overset boundary condition for the discrete adjoint variable method is presented by combining the differentiated residual equations and the objective functions on the fringe and donor cells. The automatic construction of the block connectivity among the overlap blocks is achieved by employing the overlap optimization method.

It is observed that the convergence problem of the overset adjoint solver as well as the overset flow solver, which is caused by nonconservative interpolation at the hole–fringe boundary, can also be cured by overlap optimization. To accurately evaluate the aerodynamic coefficients and to efficiently calculate the flux differentiation, the spline-boundary intersecting grid scheme is introduced. As a result, the objective function can be easily differentiated in the overlap surface. Unlike the zipper grid scheme, the interpolation of flow variables and derivatives in the overlap surface is not necessary either. The grid deformation around the overlap surfaces, such as the wing–collar and the wing–tipcap blocks, is obtained by a mapping technique from the wing surface domain to the planform domain. This mapping technique is more flexible than conventional grid perturbation in controlling local surface grid distribution.

By combining all the ingredients, an automatic design tool for shape optimization on the overset mesh system is developed, and its performance is examined through the shape design of aircraft geometries. The design results indicate that the error caused by the nonconservative interpolation at the overset boundary can be sidestepped by the overlap optimization and by suitably locating the hole–fringe boundary. Finally, the redesign of a transonic wing/body configuration successfully demonstrates the applicability of the present design approach by remarkably improving the wave drag pattern.

Acknowledgments

The authors appreciate the financial support provided by the second stage of the Brain Korea 21 Project in 2007 for Mechanical and Aerospace Engineering Research at Seoul National University, and by the Smart Unmanned Aerial Vehicle Development Program of the 21st Frontier Research and Development Program sponsored by the Ministry of Commerce, Industry, and Energy. The authors would also like to express special thanks to the Agency for Defense Development and Institute of Advanced Aerospace Technology for the financial and technical support.

References

[1] Jameson, A., "Aerodynamic Design via Control Theory," *Journal of Scientific Computing*, Vol. 3, No. 3, 1988, pp. 233–260. doi:10.1007/BF01061285

[2] Eleshaky, M. E., and Baysal, O., "Aerodynamic Shape Optimization Using Sensitivity Analysis on Viscous Flow Equations," *Journal of Fluids Engineering*, Vol. 115, No. 1, 1993, pp. 75–84. doi:10.1115/1.2910117

[3] Leoviriyakit, A., Kim, S., and Jameson, A., "Viscous Aerodynamic Shape Design Optimization of Wings Including Planform Variables," AIAA Paper 2003-3498, June 2003.

[4] Choi, S., Alonso, J. J., Kim, S., Kroo, I., and Wintzer, M., "Two-Level Multi-Fidelity Design Optimization Studies for Supersonic Jets," AIAA Paper 2005-0531, Jan. 2005.

[5] Lee, B. J., and Kim, C., "Automated Design Methodology of Turbulent Internal Flow Using Discrete Adjoint Formulation," *Aerospace Science and Technology*, Vol. 11, Nos. 2–3, 2007, pp. 163–173. doi:10.1016/j.ast.2006.12.001

[6] Nielsen, E. J., and Anderson, W. K., "Aerodynamic Design Optimization on Unstructured Meshes Using the Navier–Stokes Equations," AIAA Paper 98-4809, Sept. 1998.

[7] Kim, H. J., Sasaki, D., Obayashi, S., and Nakahashi, K., "Aerodynamic Optimization of Supersonic Transport Wing Using Unstructured Adjoint Method," *AIAA Journal*, Vol. 39, No. 6, 2001, pp. 1011–1020.

[8] Mavriplis, D. J., "Discrete Adjoint-Based Approach for Optimization Problems on Three-Dimensional Unstructured Meshes," *AIAA Journal*, Vol. 45, No. 4, 2007, pp. 741–750. doi:10.2514/1.22743

[9] Kim, C. S., Kim, C., and Rho, O. H., "Feasibility Study of Constant Eddy-Viscosity Assumption in Gradient-Based Design Optimization," *Journal of Aircraft*, Vol. 40, No. 6, 2003, pp. 1168–1176.

[10] Liao, W., and Tsai, H. M., "Aerodynamic Design Optimization by the Adjoint Equation Method on Overset Grids," AIAA Paper 2006-54, Jan. 2006.

[11] Suhs, N. E., Rogers, S. E., and Dietz, W. E., "PEGASUS 5: An Automated Preprocessor for Overset-Grid Computational Fluid Dynamics," *AIAA Journal*, Vol. 41, No. 6, 2003, pp. 1037–1045.

[12] Meakin, R. L., "Object X-rays for Cutting Holes in Composite Overset Structured Grids," AIAA Paper 2001-2537, June 2001.

[13] Noack, R. W., and Belk, D. M., "Improved Interpolation for Viscous Overset Grids," AIAA Paper 97-0199, Jan. 1997.

[14] Belk, D. M., and Maple, R. C., "Automated Assembly of Structured Grids for Moving Body Problems," AIAA Paper 95-1680, June 1995.

[15] Brown, D. L., Henshaw, W. D., and Quinlan, D. J., "Overture: Object-Oriented Tools for Overset Grid Applications," AIAA Paper 99-3130, June 1999.

[16] Chan, W. M., and Buning, P. G., "Zipper Grids for Force and Moment Computation on Overset Grids," AIAA Paper 95-1681, June 1995.

[17] Hariharan, N., Wang, Z. J., and Buning, P. G., "Application of Conservative Chimera Methodology in Finite Difference Settings," AIAA Paper 97-0627, Jan. 1997.

[18] Rumsey, C. L., and Biedron, R. T., "Computation of Flow Over a Drag Prediction Workshop Wing/Body Transport Configuration Using CFL3D," NASA TM-2001-211262, 2001.

[19] Vassberg, J. C., Buning, P. G., and Rumsey, C. L., "Drag Prediction for the DLR-F4 Wing/Body Using OVERFLOW and CFL3D on an Overset Mesh," AIAA Paper 2002-0840, Jan. 2002.

[20] Chan, W. M., Gomez, R. J., III, Rogers, S. E., and Buning, P. G., "Best Practices in Overset Grid Generation," AIAA Paper 2002-3191, June 2002.

[21] Kim, S., Kim, C., Rho, O. H., and Hong, S. K., "Cures for the Shock Instability: Development of Shock-Stable Roe Scheme," *Journal of Computational Physics*, Vol. 185, No. 2, 2003, pp. 342–374. doi:10.1016/S0021-9991(02)00037-2

[22] Jameson, A., and Yoon, S., "Lower-Upper Implicit Schemes with Multiple Grids for the Euler Equations," *AIAA Journal*, Vol. 25, No. 7, 1987, pp. 929–935. doi:10.2514/3.9724

[23] Hicks, R. M., and Henne, P. A., "Wing Design by Numerical Optimization," *Journal of Aircraft*, Vol. 15, No. 7, 1978, pp. 407–412. doi:10.2514/3.58379

[24] Martins, J. R. R. A., Kroo, I. M., and Alonso, J. J., "Automated Method for Sensitivity Analysis Using Complex Variables," AIAA Paper 2000-0869, Jan. 2000.

[25] Fletcher, R., and Powell, M. J. D., "Rapidly Convergent Descent Method for Minimization," *Computer Journal*, Vol. 6, No. 2, 1963, pp. 163–168.